Nanoscale Optical Properties of Indium Gallium Nitride/Gallium Nitride Nanodisk-in-Rod Heterostructures

Xiang Zhou,[†] Ming-Yen Lu,[‡] Yu-Jung Lu,[§] Eric J. Jones,[†] Shangjr Gwo,[§] and Silvija Gradečak*,[†]

[†]Department of Materials Science and Engineering, Massachusetts Institute of Technology, Cambridge, Massachusetts 02139, United States, [‡]Graduate Institute of Opto-Mechatronics, National Chung Cheng University, Chia-Yi 62102, Taiwan, and [§]Department of Physics, National Tsing Hua University, Hsinchu 30013, Taiwan

ABSTRACT III-nitride based nanorods and nanowires offer great potential for optoelectronic applications such as light emitting diodes or nanolasers. We report nanoscale optical studies of InGaN/GaN nanodisk-in-rod heterostructures to quantify uniformity of light emission on the ensemble level, as well as the emission characteristics from individual InGaN nanodisks. Despite the high overall luminescence efficiency, spectral and intensity inhomogeneities were observed and directly correlated to the compositional variations among nanodisks and to the presence of structural defect, respectively. Observed light quenching is correlated to type I1 stacking faults in InGaN nanodisks, and the mechanisms for stacking fault induced nonradiative recombinations are discussed in the context of band structure around stacking faults and Fermi level pinning at nanorod surfaces. Our results highlight the importance of controlling III-nitride nanostructure growths to further reduce defect formation and ensure compositional homogeneity for optoelectronic devices with high efficiencies and desirable spectrum response.

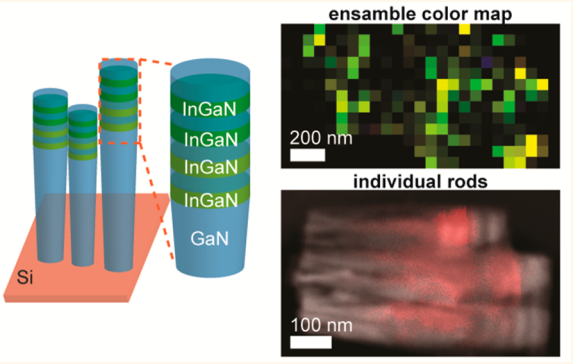

KEYWORDS: III-nitrides · nanowires · nanorods · cathodoluminescence · optical properties

The III-nitride nanorods, nanowires and their heterostructures have attracted significant research interest for a range of electronic and optoelectronic applications due to their dislocation-free structure,[1,2] effective strain relaxation on lattice mismatched substrates,[3,4] as well as waveguiding and light trapping properties.[5,6] A number of nitride nanowire and nanorod based devices, including transistors,[7] light emitting diodes (LEDs),[8,9] lasers,[10,11] photodetectors,[12] and solar cells[13] have been demonstrated on both individual and ensemble nanorod level. The realization of these nanorod-based devices and their performances rely on effective and controlled doping and alloying. In particular, effective control over indium alloying with gallium nitride is essential to achieve high-performance devices based on InGaN/GaN nanorod heterostructures with high efficiencies and precise spectrum tuning. On the ensemble level, control over the uniformity of indium composition on the macroscopic scale is required to make either monochromatic LEDs with narrow spectral emission or white LEDs through balanced color mixing. On the individual nanorod level, defect-free and chemically homogeneous InGaN layers (shells or disks) are important to reduce nonradiative recombination and maintain high efficiency. To further improve the performance of nanorod-based LED devices, a better understanding of the structure, composition, defects and optical properties on the nanometer scale is critical.

Here, we report on nanoscale structure, composition, and optical properties correlation in ensemble and individual InGaN/GaN nanodisk-in-rod heterostructures, using cathodoluminescence in scanning transmission electron microscopy (CL-STEM).[14] While previous studies on different semiconductor nanowire heterostructures, such as InGaN/GaN,[15] AlN/GaN,[16] ZnO/ZnS,[17,18] and GaAs/AlGaAs/GaAs,[19] focus mostly on individual nanostructures, in this work we focus on structure-optical property correlation on

* Address correspondence to gradecak@mit.edu.

Received for review December 2, 2014 and accepted February 7, 2015.

Published online February 07, 2015
10.1021/nn506867b

© 2015 American Chemical Society

both micro- and nanoscale. We provide direct visualization and quantification of homogeneity of indium incorporation and resulting nanorod emission. In addition, by investigating individual nanorods and InGaN nanodisks, we identified type I1 stacking faults as the main source of nonradiative recombination in InGaN nanodisks. Our results provide important insights for further improvement of the design, fabrication, and performance of III-nitride nanowire/rod based optoelectronic devices.

InGaN/GaN nanodisk-in-rod heterostructures were grown by plasma-assisted molecular beam epitaxy (PAMBE), as reported previously.[9,20] Si-doped GaN nanorod arrays of about 300 nm height were first grown on a Si(111) substrate at 770 °C, after which indium was introduced periodically to form InGaN nanodisks of 15−25 nm in thickness. The nominal nanodisk composition was controlled by varying the growth temperature (ranging from 690 to 705 °C, corresponding to highest and lowest amount of indium, respectively) and the ratio of indium to gallium content. The nanodisks were capped with GaN barrier layer grown at 690−700 °C. In some cases, due to limited mobility of indium adatoms on the growth facet, the InGaN nanodisk were also capped by a GaN shell in the radial direction. The main focus of this study is on GaN nanorods with 4 InGaN nanodisks tailored for green and red emission: the first two nanodisks were targeted for green emission (nominal In composition of 20−30%) and the last two for red emission (nominal In composition of 40%). For comparison, nanorods with one and two nanodisks and grown under different growth conditions will also be discussed.

RESULTS AND DISCUSSIONS

The scanning electron microscopy (SEM) image of the InGaN/GaN nanodisk-in-rod heterostructures with 4 InGaN nanodisks is shown in Figure 1a and the corresponding schematic of the structure is illustrated in Figure 1b. The average length of the nanorods is ~500 nm with general inverse tapering observed from the bottom to the top of the nanorods (diameters ~50 and ~200 nm, respectively), with some degree of coalescence. The presence of four InGaN nanodisks was confirmed by STEM (Figure 1c). The ensemble optical properties of the nanorods were investigated by photoluminescence (PL) at room temperature (Figure 1d). A GaN-related emission band centered at 3.41 eV and a relatively broad emission InGaN band at 2.30 eV were observed. A separate PL measurement using a 532 nm excitation source and InGaAs detector (not shown) exhibit no additional emission peaks for wavelengths longer than 700 nm, ruling out the possibility of any infrared emission from more In-rich InGaN nanodisks. The peak positions from the InGaN nanodisk emission vary slightly across the substrate, in the range of 2.28−2.34 eV, with a full width at

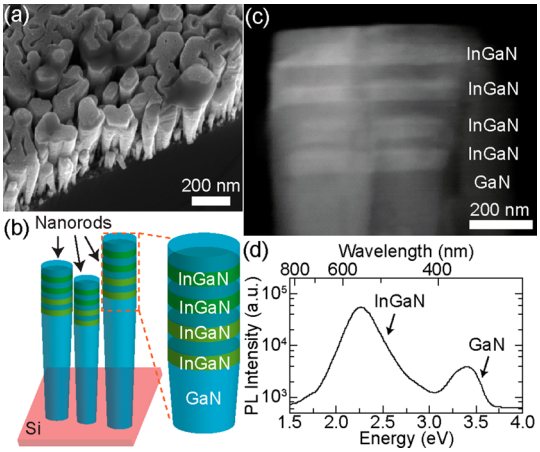

Figure 1. (a) SEM micrograph of InGaN/GaN nanodisk-in-rod nanorod arrays grown on silicon substrate (45° tilted view) and (b) the corresponding schematic of the structure. (c) Dark field STEM image of the nanodisk-in-rod heterostructures showing four InGaN nanodisks near the nanorod top. InGaN nanodisks appear as brighter regions due to higher Z-contrast. (d) Representative PL spectrum (log scale) from an ensemble of nanorods showing GaN- and InGaN-related peaks.

half-maximum (fwhm) of 270 meV (see Supporting Information, Figure S1). The spread of the peak positions and their widths are likely due to compositional inhomogeneities from a large number of nanodisks studied during the ensemble measurements.

The microscopic PL measurements indicate that individual nanorods on the substrate level can have very distinct optical properties, although they are grown at the same time. To investigate the nanoscale optical properties and the source of these inhomogeneities, nanorods were removed from the growth substrate by sonication and drop cast onto lacey carbon covered copper grids for transmission electron microscopy (TEM) and CL-STEM investigations. First, micrometer-size clusters of nanorods standing up on the TEM grid (Supporting Information, Figure S2) were investigated to probe the uniformity of optical emission from individual nanorod heterostructures over a large area. Figures 2a,b shows the dark field STEM and corresponding panchromatic CL images of the nanorod cluster in top-down geometry, collected at 96 K. From the CL images it can be observed that the CL intensity from individual nanorods is not homogeneous across the sample; a number of nanorods have very bright CL emission, while some nanorods show almost no CL signal. The CL spectrum of the nanorod ensemble (Figure 2c) also shows a broad emission peak from InGaN nanodisks centered at 2.28 eV, which is qualitatively consistent with the PL result. However, by collecting monochromatic images on the same nanorod ensemble at energies of 2.48, 2.36, and 2.28 eV (Figure 2d−f), nanoscale inhomogeneous emission can be observed from individual nanorods that cannot be resolved using PL. For example, in the

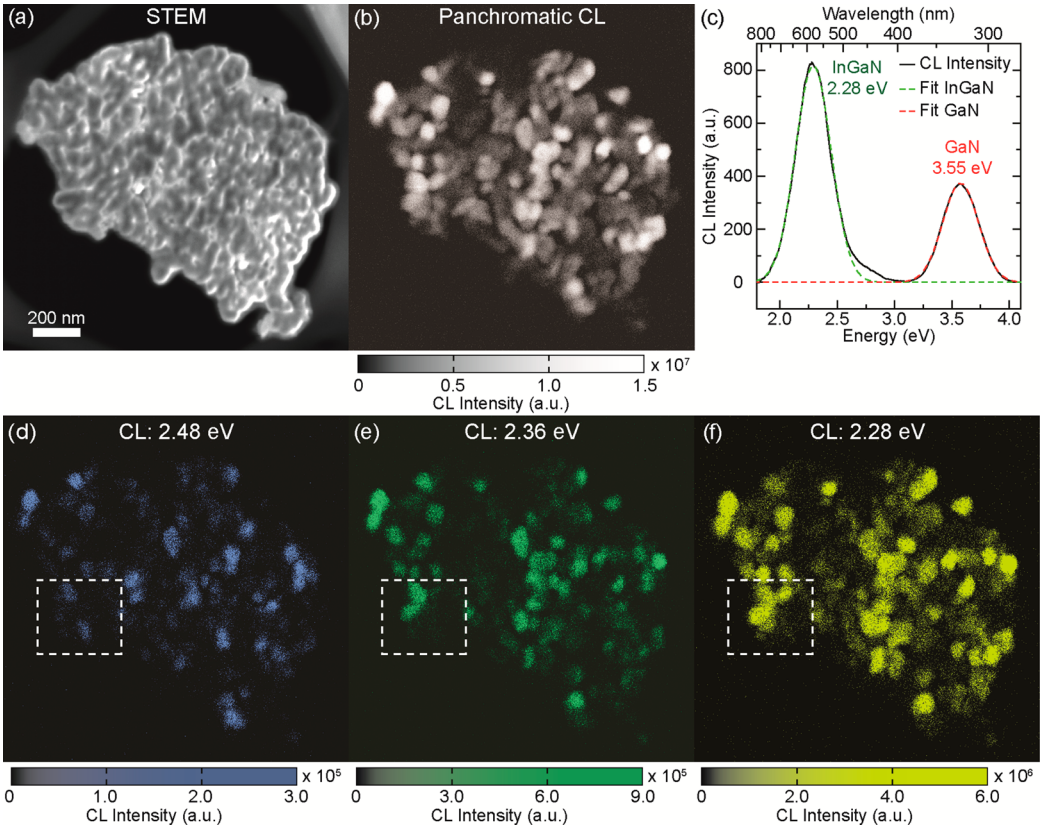

Figure 2. CL mapping of InGaN/GaN nanodisk-in-rod ensemble. (a) Dark field STEM and (b) corresponding panchromatic CL images of the same nanorod ensemble standing up on the TEM grid, as shown in Figure 1c. (c) CL spectrum (96 K) of the nanorod ensemble, showing emissions from both InGaN (2.28 eV) and GaN (3.55 eV), with respective Gaussian peak fittings. (d–f) Monochromatic CL images of the same nanorod ensemble shown in (a), taken at 2.48, 2.36, and 2.28 eV. The boxed region highlights that neighboring nanorods that have different peak CL emission wavelengths. CL intensities bars for (b) and (d–f) are included below the figure. All STEM and CL images shared the same scale shown in (a). The sample geometry is described in Supporting Information Figure S2.

boxed region in Figure 2d–f, neighboring nanorods show distinct emission energies indicating different nanodisk compositions, which in turn determine the corresponding band gap.

To investigate properties of a nanorod ensemble used to make larger-scale devices, while achieving a sufficient spatial resolution to distinguish individual nanorods, hyperspectral CL imaging was performed with parallel spectrum acquisition using a CCD camera, where each scanning pixel contains a full CL spectrum (Figure 3). A pixel size of 60 nm was chosen to match the observed nanorod diameters, such that one pixel approximately matches the size of a single nanorod. While no CL emission was observed from a number of nanorods, up to three different CL emission peaks can be observed from individual pixels that were fitted with Gaussian peaks to extract emission energy and intensity (sample CL spectra from the spectrum image and the peak statistics are shown in the Supporting Information, Figures S3 and S4). The values of fitted CL peak energies span from 1.9 to 2.8 eV with an average fwhm of 0.14 eV, which is much sharper compared to the CL spectrum on the cluster shown in Figure 2c. By summing the fitted peaks, we verified that the sum

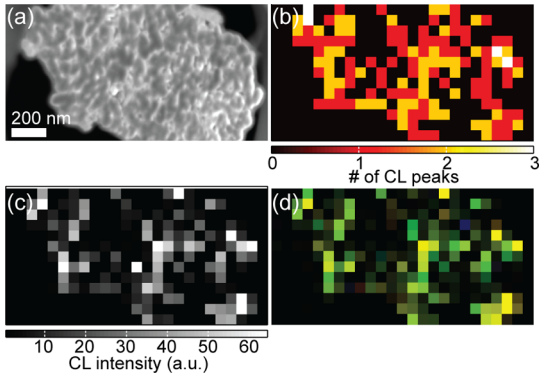

Figure 3. CL color mapping of InGaN-GaN nanodisk-in-rod ensemble. (a) Dark field STEM image of the nanorod ensemble standing up on TEM grid. (b) Corresponding map showing the number of CL emission peaks across the sample. (c) CL integrated intensities obtained by summing intensities of individual Gaussian-fitted peaks for each pixel. (d) Calculated color map of the nanorod ensemble based on the CL spectrum image. Statistics of the spectrum imaging results is available in Figures S3–S5 in Supporting Information.

spectrum coincides with the ensemble spectrum (see Supporting Information, Figure S5). These results indicate that we are detecting emission from individual, well-defined nanodisks that collectively contribute to

the assembly emission. By extracting emission color from individual nanorods, we calculated the color and intensity maps (Figure 3) giving us a direct way of visualizing the homogeneity of CL emissions from the nanorod ensemble. From the color map, it can be seen that the majority of the nanorods emit green or yellow light, while only several of them emit blue and red. The spectral uniformity depends on the homogeneity of indium content in the active InGaN nanodisks across multiple nanorods. On the basis of the statistics of CL peak fitting results and a band gap bowing parameter of 1.43,[21] the average indium compositions across multiple nanorods is 30% ± 5% and the total range of CL emission energies indicated maximum compositional inhomogeneity of ±10%. For monochromatic LED devices, a uniform indium composition is desired to narrow down the emission spectrum, while for white LED devices, an appropriate mix of indium compositions is required to tune the blue, green, and red lighting component. Our results are the first direct demonstration that for a nanorod ensemble grown at predefined identical conditions, there are substantial differences in indium composition across neighboring nanorods, which cause spectrum broadening observed in larger-scale investigations. This finding is surprising for materials grown using a MBE system, where near equilibrium growth conditions and slow growth rates provide excellent control in stoichiometry and chemical composition in thin films of complex compositions. Improved reactor design, tuning of growth parameters, and/or improving uniformity or nanorod size and density will be required to finely control the indium incorporation and resulting emission uniformity for nanorod arrays on a larger scale.

Interestingly, a majority of nanorods investigated in Figures 2 and 3 have one or two well-defined CL emission peaks from a total of four InGaN nanodisks, implying that not all InGaN nanodisks are efficient light emitters. To study preferential CL emission or quenching in individual nanodisks, nanorods lying sideways on the TEM grid were investigated next. Figure 4a shows an overlay of the panchromatic CL intensity signal (red) and the corresponding STEM image (gray) from several representative individual nanorods containing InGaN nanodisks. It can be observed that at most 2 out of 4 InGaN nanodisks from each nanorod have a strong CL emission, whereas CL quenching is always observed in the top two nanodisks. This result was further confirmed by obtaining a CL line scan along one of the nanorods (Figure 4b) where two CL emission peaks centered at 2.40 and 2.25 eV were observed from the first two InGaN nanodisks. We note that the CL emission can be observed along a 50 nm length on the line scan, which is larger than the 15−20 nm estimated thickness of the nanodisks, due to carrier diffusion into the nanodisks; even when the point of electron beam excitation is in the GaN barrier

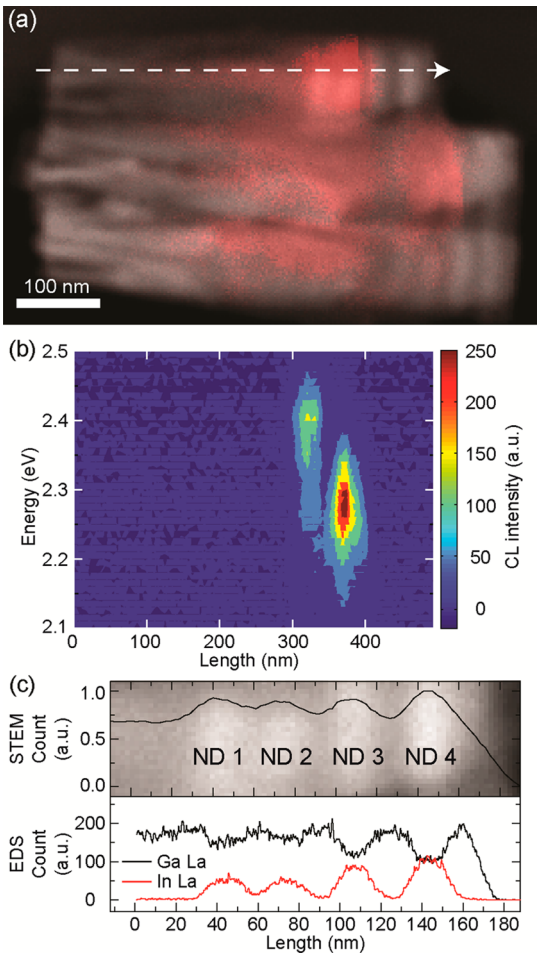

Figure 4. (a) Overlay of panchromatic CL image (red) onto STEM image (gray) of individual nanorods and nanodisks, showing only two out of four nanodisks emit CL strongly. (b) CL spectrum image obtained from a line scan along a nanorod, as illustrated by the white arrow in (a), confirming CL emissions with two different energies from individual nanodisks. (c) STEM image (top) with the corresponding intensity profile (overlaid) and EDS line profiles for Ga and In (bottom).

layers, some of the carriers diffuse and recombine in the InGaN nanodisks. The fwhm's of the observed CL emission peaks fluctuate between 110 and 190 meV, consistent with the values reported from spectrum imaging results, and indicating that the observed emissions are truly from individual nanodisks. The observed difference in the position of the CL emission peaks are due to differences in local indium compositions inside the two InGaN nanodisks, which was confirmed by energy dispersive X-ray spectroscopy (EDS) line scan shown in Figure 4c. Quantitative EDS analysis confirm that the first two nanodisks grown (1 and 2) contain 15−20% indium, while the other two nanodisks contain about 30% indium, but the EDS quantification underestimates the indium composition due to a GaN shell capping the nanodisks. In addition, it is also observed that the intensity of CL emission from the first nanodisk is significantly lower than from the second

nanodisk. Notably, this trend is observed across multiple nanorods. In fact, in a large percentage of nanorods investigated, only one CL emission is observed from the second nanodisk, while no emission was observed from the other three nanodisks. This result is consistent with the nanorod emission statistics shown in Figure 3b, as a majority of the nanorods were shown to be either nonemitting or emitting CL of only one wavelength.

CL quenching in InGaN nanodisks implies that not every nanodisk is an efficient light emitter for optoelectronic applications. The observation that not all of the InGaN disk-like insertions inside PAMBE grown GaN nanorods emit light has been reported by Toubot *et al.*[22] However, to date there is no systematic study on the exact cause of CL quenching in InGaN/GaN nanorod heterostructures. Understanding the root cause for nonradiative recombination in the active layers of InGaN is critical for evaluating and improving the performances of LED devices made from nanowire and nanorod heterostructures, but also of InGaN/GaN heterostructures in general. In what follows, we show that the preferential CL quenching in specific nanodisks is closely related to the presence of structural defects.

Bright field TEM imaging (Figure 5a) was performed to investigate the structural quality of the same nanodisks shown in Figure 4. Multiple basal plane stacking faults were observed extending through the entire width of the nanorods. In addition, significantly more stacking faults were observed in nanodisks 3 and 4 (more than 15) compared to nanodisks 1 and 2 (no stacking faults were observed within nanodisks), suggesting that such defects are a major factor in light quenching. The stacking faults can be classified as type I1, with an ABABCBCB... stacking sequence, as determined using high angle annular dark field (HAADF) STEM (Figure 5b). This type of stacking fault has the lowest formation energy for III-nitride systems (10 and 19 meV per unit cell for GaN and InN, respectively), and they are largely related to instabilities in growth conditions instead of strain as their formation cannot relax strain.[23] No other type of defects, such as dislocations or grain boundaries, were observed from TEM studies of multiple similar samples, indicating that stacking faults are the main type of defects in these nanorods and nanodisks. On the other hand, bright CL emission could be observed from both nanodisks if neither of them contain stacking faults. As shown in Figure 6, two bright CL emissions centered at 2.65 and 2.85 eV could be observed from two neighboring nanodisks, with their emission energies tuned by the relative amount of indium (the upper nanodisk emits photons of higher energy as it contains less indium). Bright field TEM study verified that in this case there are no stacking faults in either of the nanodisks. In addition, we also confirm that for GaN nanorods with one InGaN

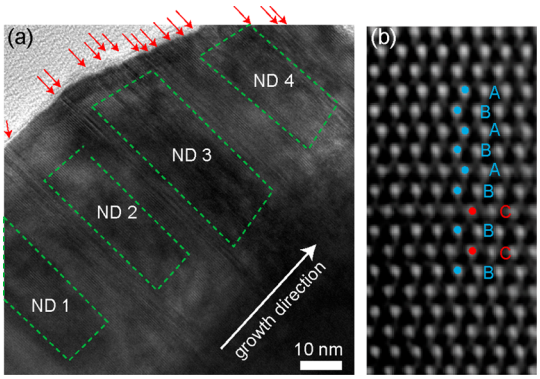

Figure 5. TEM structural analysis of InGaN nanodisks. (a) Bright field TEM image of the same InGaN nanodisks (labeled ND 1 to ND 4) investigated in Figure 4. Line contrasts perpendicular to the growth direction are stacking faults, which are indicated by red arrows. (b) Aberration-corrected dark field STEM image of a stacking fault in InGaN. Different atomic planes are labeled as A, B, and C in the figure for visualization of type I1 stacking fault (ABABCBCB... stacking).

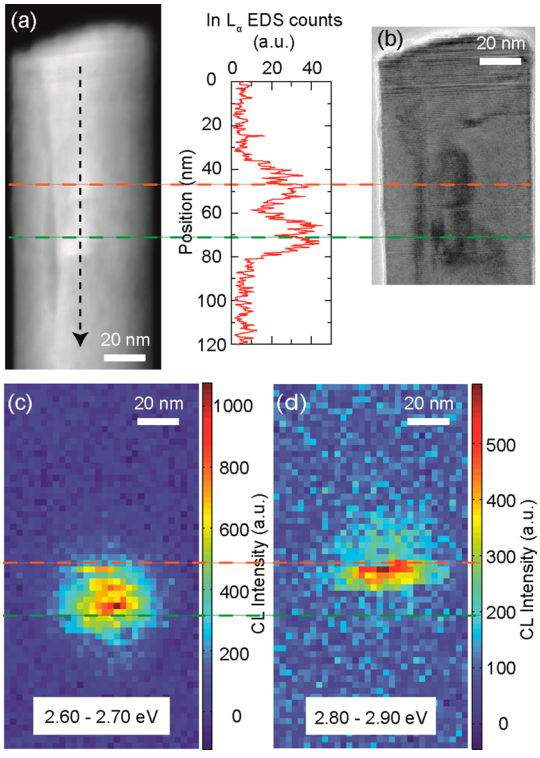

Figure 6. Example of CL emission without quenching from a nanorod containing two nanodisks without stacking faults. (a) STEM image and corresponding EDS In profile of a GaN nanorod with two InGaN nanodisks embedded. (b) Corresponding high resolution TEM image taken along the $\langle 11\bar{2}0 \rangle$ zone axis demonstrating an absence of stacking faults inside the nanodisks. (c and d) Integrated CL intensity maps (2.60−2.70 and 2.80−2.90 eV, respectively) of the same nanodisks, with a 4 nm spatial resolution and 1 nm spectral resolution obtained from spectrum imaging, showing CL emissions from both nanodisks. The orange and green lines are for visual aid to indicate the position of the two InGaN nanodisks.

nanodisk (~7% In), the quenching of light emission is related to the presence of stacking faults, as shown in

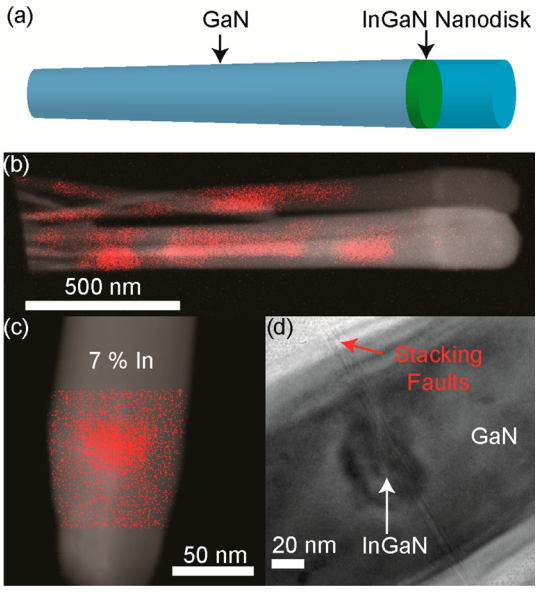

Figure 7. Stacking fault related CL quenching in GaN nanorod with one InGaN nanodisk. (a) Schematic representation of nanodisk-in-rod structure. (b) Panchromatic CL (red) map overlaid on the corresponding STEM image (gray), of a GaN nanorod containing only one InGaN nanodisk seen as a bright vertical strip at about 150 nm from the nanorod top. No CL emission was observed from the InGaN nanodisk region. (c) EDS indium map (red) of an InGaN nanodisk overlaid on the corresponding STEM image (gray). (d) High resolution TEM image showing stacking faults cutting through the InGaN nanodisk.

Figure 7. CL-STEM and TEM studies of similar InGaN/GaN nanodisk-in-rod samples with different number (2, 4, and 5) of nanodisks show the same trend of CL quenching in InGaN disks with the presence of stacking faults (Supporting Information, Figures S6–S9). The stacking faults are mostly likely formed when temperature is lowered and indium is introduced for the formation of InGaN nanodisks, which induces fluctuations in nucleation and adatom diffusion lengths, as well as other thermodynamic and kinetic parameters.

Stacking faults and zinc blend domains have been reported in GaN based nanowires, nanorods, and heterostructures grown by both seed particle-mediated or particle free-methods[24−26] and low device efficiency of nonpolar GaN thin film devices are often related to high stacking fault densities,[27,28] but without direct evidence. In GaN thin film geometries, luminescence quenching by stacking faults is often associated with partial dislocations where the stacking faults end.[27] In the nanorods that we studied, most stacking faults were observed to propagate along the entire diameter of the nanorod, terminating at the edges or side walls (Supporting Information, Figure S10). This implies that the stacking faults are pinned to the nanorod sidewall, and no partial dislocations inside InGaN/GaN nanorods were observed. An alternative approach to probe the light quenching mechanism by stacking faults is by examining the electronic structure around the stacking faults. Stacking faults in III nitrides are usually modeled as a thin layer of zincblende phase (with ABCABC... stacking) in contact with the wurtzite phase (with ABAB... stacking). For type I1 stacking faults in thin films, a type II band alignment, in which both the conduction and valence bands of wurtzite phase are higher than the zincblende phase, has been theoretically predicted[23] and speculated from experimental results.[29] Such band alignment could result in spatial separation of electron and holes once they are excited in the material.[29] In addition, spontaneous and piezoelectric polarizations along ⟨0002⟩ direction in wurtzite nitrides can also induce a large built-in electric field across the zincblende domain or stacking fault,[30,31] thus further reducing the radiative recombination rate. Besides the issue of band alignment at the stacking faults, Fermi level pinning and the resulting electric field set up in GaN nanorods[32,33] could lead to further charge separation, especially for diameters below 100 nm. Electrons and holes excited by the electron beam can be first separated across the stacking faults, and move further apart under the electric field due to Fermi level pinning. Specific studies focused on InGaN nanostructures should provide additional insights on the role of stacking faults on their optical emissions.

CONCLUSION

In conclusion, structure−property correlation was performed on InGaN/GaN nanodisk-in-rod heterostructures with nanometer resolution on both the ensemble and individual nanorod levels. The ensemble measurements show inhomogeneity in both emission intensity and wavelengths from individual nanorods in a micrometer sized cluster, indicating differences in defect densities and indium concentrations in the active layers. On the individual nanodisk and nanorod level, quenching of the CL emission was directly correlated to the presence of growth-related type I1 stacking faults inside the InGaN nanodisks. CL quenching mechanism was related to the electronic band structure around the stacking faults, as well as Fermi level pinning associated with the unpassivated surface. These results are significant for the development of nanowire- and nanorod-based LED devices. On an ensemble level, spectral uniformity and mixing are determined by the indium compositions in the active layer, and are essential for monochromatic or white light emissions. On the nanometer scale, our results indicate that avoiding the formation of defects such as stacking faults and proper surface passivation will be important for further improvement in device efficiencies, especially at room or device operation temperatures. These results also highlight the importance of controlling III-nitride nanostructure growths in MBE

to further reduce defect formation and ensure compositional homogeneity for optoelectronic devices with high efficiencies and desirable spectrum response.

METHODS

The InGaN/GaN nanorod array were grown on 3-in., Si(111) wafers by nitrogen-plasma-assisted molecular beam epitaxy (PAMBE) under nitrogen-rich conditions. Prior to the InGaN nanodisk growth, vertically aligned Si-doped n-GaN nanorod arrays (~300 nm in height) were grown first on the Si(111) substrate at 770 °C (growth temperature as the nanorod growth template). Subsequently, InGaN nanodisks were self-organized on top of the n-type GaN nanorods. For the nanorods with four InGaN nanodisks, a growth temperature of 700 °C was used to grow the first two nanodisks, with In/Ga flux ratio of 1.2. Temperature was decreased to 670 and 650 °C, with In/Ga flux ratio of 1.85 and 2.52 to grow the third and fourth nanodisks, respectively. Nevertheless, the In compositions in the third and fourth InGaN nanodisks revealed by X-ray diffraction and EDS were very similar.

CL-STEM measurements were performed on a JEOL 2011 TEM operating at 120 kV, coupled with a Gatan MONOCL3+ system. The electron probe size is on the order of 1 nm, while the spectral resolution for spectrum imaging was 1 nm (0.25 nm with 4 times spectrum binning). The nanorods samples were prepared by sonication of the growth substrate in ethanol followed by drop casting on to carbon lacey TEM grids. TEM samples were cooled to 96 K by liquid nitrogen. High resolution bright field, dark field TEM images and STEM-EDS mapping were obtained from a JEOL 2010F TEM operated at 200 kV. Aberration corrected STEM images for stacking faults analysis were using a JEOL JEM ARM 200F TEM operated at 200 kV with spherical aberration corrector. PL measurements were performed using a home-built photoluminescence system with 262 nm excitation laser (CrystaLaser, Nd:YLF). Finite element analysis were performed using ADINA software.

Conflict of Interest: The authors declare no competing financial interest.

Supporting Information Available: CL mapping statistics on ensemble of InGaN/GaN nanorods, CL, TEM, and EDS correlation on nanorods containing different number of InGaN nanodisks. This material is available free of charge *via* the Internet at http://pubs.acs.org.

Acknowledgment. This work is funded by the Center for Excitonics, Energy Frontier Research Center funded by the U.S. Department of Energy, Office of Basic Energy Sciences under Award Number DE-SC0001088. The authors acknowledge the use of the MRSEC Shared Experimental Facilities at MIT, supported by the National Science Foundation under award number DMR-08-19762. M. Lu, Y. Lu and S. Gwo also acknowledge support from the Ministry of Science and Technology in Taiwan (MOST-103-2628-M-007-001 and MOST 103-2221-E-194 -050 -MY2). We would like to thank Dr. Yong Zhang and Dr. Shiahn Chen for their technical assistance.

REFERENCES AND NOTES

1. Duan, X.; Lieber, C. Laser-Assisted Catalytic Growth of Single Crystal GaN Nanowires. *J. Am. Chem. Soc.* **2000**, *122*, 188–189.
2. Tu, L. W.; Hsiao, C. L.; Chi, T. W.; Lo, I.; Hsieh, K. Y. Self-Assembled Vertical GaN Nanorods Grown by Molecular-Beam Epitaxy. *Appl. Phys. Lett.* **2003**, *82*, 1601.
3. Xiang, H.; Wei, S.-H.; Da Silva, J.; Li, J. Strain Relaxation and Band-Gap Tunability in Ternary InxGa1−xN Nanowires. *Phys. Rev. B* **2008**, *78*, 193301.
4. Glas, F. Critical Dimensions for the Plastic Relaxation of Strained Axial Heterostructures in Free-Standing Nanowires. *Phys. Rev. B* **2006**, *74*, 121302.
5. Yan, R.; Gargas, D.; Yang, P. Nanowire Photonics. *Nat. Photonics* **2009**, *3*, 569–576.
6. Chesin, J.; Gradecak, S. Comparing Directed Efficiency of III-Nitride Nanowire Light-Emitting Diodes. *J. Nanophotonics* **2014**, *8*, 083095.
7. Huang, Y.; Duan, X.; Cui, Y.; Lieber, C. M. Gallium Nitride Nanowire Nanodevices. *Nano Lett.* **2002**, *2*, 101–104.
8. Qian, F.; Gradecak, S.; Li, Y.; Wen, C.-Y. Y.; Lieber, C. M. Core/multishell Nanowire Heterostructures as Multicolor, High-Efficiency Light-Emitting Diodes. *Nano Lett.* **2005**, *5*, 2287–2291.
9. Lin, H.-W.; Lu, Y.-J.; Chen, H.-Y.; Lee, H.-M.; Gwo, S. InGaN/GaN Nanorod Array White Light-Emitting Diode. *Appl. Phys. Lett.* **2010**, *97*, 073101.
10. Johnson, J. C.; Choi, H.-J.; Knutsen, K. P.; Schaller, R. D.; Yang, P.; Saykally, R. J. Single Gallium Nitride Nanowire Lasers. *Nat. Mater.* **2002**, *1*, 106–110.
11. Lu, Y.-J.; Kim, J.; Chen, H.-Y.; Wu, C.; Dabidian, N.; Sanders, C. E.; Wang, C.-Y.; Lu, M.-Y.; Li, B.-H.; Qiu, X.; et al. Plasmonic Nanolaser Using Epitaxially Grown Silver Film. *Science* **2012**, *337*, 450–453.
12. Rigutti, L.; Tchernycheva, M.; De Luna Bugallo, A.; Jacopin, G.; Julien, F. H.; Zagonel, L. F.; March, K.; Stephan, O.; Kociak, M.; Songmuang, R. Ultraviolet Photodetector Based on GaN/AlN Quantum Disks in a Single Nanowire. *Nano Lett.* **2010**, *10*, 2939–2943.
13. Tang, Y. B.; Chen, Z. H.; Song, H. S.; Lee, C. S.; Cong, H. T.; Cheng, H. M.; Zhang, W. J.; Bello, I.; Lee, S. T. Vertically Aligned P-Type Single-Crystalline GaN Nanorod Arrays on N-Type Si for Heterojunction Photovoltaic Cells. *Nano Lett.* **2008**, *8*, 4191–4195.
14. Lim, S. K.; Brewster, M.; Qian, F.; Li, Y.; Lieber, C. M.; Gradecak, S. Direct Correlation between Structural and Optical Properties of III-V Nitride Nanowire Heterostructures with Nanoscale Resolution. *Nano Lett.* **2009**, *9*, 3940–3944.
15. Lähnemann, J.; Hauswald, C.; Wölz, M.; Jahn, U.; Hanke, M.; Geelhaar, L.; Brandt, O. Localization and Defects in Axial (In,Ga)N/GaN Nanowire Heterostructures Investigated by Spatially Resolved Luminescence Spectroscopy. *J. Phys. D: Appl. Phys.* **2014**, *47*, 394010.
16. Tizei, L. H. G.; Meuret, S.; March, K.; Hestroffer, K.; Auzelle, T.; Daudin, B.; Kociak, M. A Polarity-Driven Nanometric Luminescence Asymmetry in AlN/GaN Heterostructures. *Appl. Phys. Lett.* **2014**, *105*, 143106.
17. Liu, H.; Hu, L.; Watanabe, K.; Hu, X.; Dierre, B.; Kim, B.; Sekiguchi, T.; Fang, X. Cathodoluminescence Modulation of ZnS Nanostructures by Morphology, Doping, and Temperature. *Adv. Funct. Mater.* **2013**, *23*, 3701–3709.
18. Yan, J.; Fang, X.; Zhang, L.; Bando, Y. Structure and Cathodoluminescence of Individual ZnS/ZnO Biaxial Nanobelt Heterostructures. *Nano Lett.* **2008**, *8*, 2794–2799.
19. Estrin, Y.; Rich, D.; Kretinin, A.; Shtrikman, H. Of Metal Deposition on Exciton−Surface Plasmon Polariton Coupling in GaAs/AlAs/GaAs Core−Shell Nanowires Studied with Time-Resolved Cathodoluminescence. *Nano Lett.* **2013**, *13*, 1602–1610.
20. Lu, Y.-J.; Lin, H.-W.; Chen, H.-Y.; Yang, Y.-C.; Gwo, S. Single InGaN Nanodisk Light Emitting Diodes as Full-Color Subwavelength Light Sources. *Appl. Phys. Lett.* **2011**, *98*, 233101.
21. Wu, J.; Walukiewicz, W. Band Gaps of InN and Group III Nitride Alloys. *Superlattices Microstruct.* **2003**, *34*, 63–75.
22. Tourbot, G.; Bougerol, C.; Glas, F.; Zagonel, L. F.; Mahfoud, Z.; Meuret, S.; Gilet, P.; Kociak, M.; Gayral, B.; Daudin, B. Growth Mechanism and Properties of InGaN Insertions in GaN Nanowires. *Nanotechnology* **2012**, *23*, 135703.
23. Stampfl, C.; Van de Walle, C. G. Energetics and Electronic Structure of Stacking Faults in AlN, GaN, and InN. *Phys. Rev. B* **1998**, *57*, R15052–R15055.

24. Tham, D.; Nam, C.-Y.; Fischer, J. E. Defects in GaN Nanowires. *Adv. Funct. Mater.* **2006**, *16*, 1197–1202.
25. Zhou, X.; Chesin, J.; Crawford, S.; Gradečak, S. Using Seed Particle Composition to Control Structural and Optical Properties of GaN Nanowires. *Nanotechnology* **2012**, *23*, 285603.
26. Kehagias, T.; Dimitrakopulos, G. P.; Becker, P.; Kioseoglou, J.; Furtmayr, F.; Koukoula, T.; Häusler, I.; Chernikov, a; Chatterjee, S.; Karakostas, T.; et al. Nanostructure and Strain in InGaN/GaN Superlattices Grown in GaN Nanowires. *Nanotechnology* **2013**, *24*, 435702.
27. Wu, F.; Lin, Y.-D.; Chakraborty, A.; Ohta, H.; DenBaars, S. P.; Nakamura, S.; Speck, J. S. Stacking Fault Formation in the Long Wavelength InGaN/GaN Multiple Quantum Wells Grown on M-Plane GaN. *Appl. Phys. Lett.* **2010**, *96*, 231912.
28. Lin, Y.-D.; Chakraborty, A.; Brinkley, S.; Kuo, H. C.; Melo, T.; Fujito, K.; Speck, J. S.; DenBaars, S. P.; Nakamura, S. Characterization of Blue-Green M-Plane InGaN Light Emitting Diodes. *Appl. Phys. Lett.* **2009**, *94*, 261108.
29. Lu, X. H.; Yu, P. Y.; Zheng, L. X.; Xu, S. J.; Xie, M. H.; Tong, S. Y. Evidence for a Type-II Band Alignment between Cubic and Hexagonal Phases of GaN. *Appl. Phys. Lett.* **2003**, *82*, 1033–1035.
30. Metcalfe, G. D.; Shen, H.; Wraback, M.; Hirai, A.; Wu, F.; Speck, J. S. Enhanced Terahertz Radiation from High Stacking Fault Density Nonpolar GaN. *Appl. Phys. Lett.* **2008**, *92*, 241106.
31. Liu, L. Z.-Y.; Rao, D. V. S.; Kappers, M. J.; Humphreys, C. J.; Geiger, D. Basal-Plane Stacking Faults in Non-Polar GaN Studied by off-Axis Electron Holography. *J. Phys. Conf. Ser.* **2010**, *209*, 012012.
32. Cavallini, A.; Polenta, L.; Rossi, M.; Stoica, T.; Calarco, R.; Meijers, R. J.; Richter, T.; Lüth, H. Franz−Keldysh Effect in GaN Nanowires. *Nano Lett.* **2007**, *7*, 2166–2170.
33. Calarco, R.; Marso, M.; Richter, T. Size-Dependent Photoconductivity in MBE-Grown GaN-Nanowires. *Nano Lett.* **2005**, *5*, 981–984.